Frequency domain analysis of the linearized Navier-Stokes equations

Mihailo R. Jovanović
jmihailo@engineering.ucsb.edu

Bassam Bamieh
bamieh@engineering.ucsb.edu

Department of Mechanical and Environmental Engineering
University of California, Santa Barbara, CA 93106-5070

Abstract

We study the Linearized Navier-Stokes (LNS) equations from an input-output point of view by analyzing their spatio-temporal frequency responses. We show how the relative roles of Tollmien-Schlichting (TS) waves and streamwise vortices and streaks can be explained as input-output resonances of the spatio-temporal frequency responses. Furthermore, we derive important conclusions about the effectiveness of input field components, and the contributions of the streamwise, wall-normal, and spanwise velocity perturbations to the kinetic energy density. In particular, we show that the wall-normal and spanwise forces have much stronger influence on the velocity field than the streamwise force. On the other hand, the velocity perturbations in the direction of a nominal flow achieve much bigger magnitudes than the perturbations in the other two spatial directions.

1 Introduction

In this paper, we analyze the dynamical properties of the Navier-Stokes (NS) equations with spatially distributed and temporally varying body force fields. These fields are considered as inputs, while various combinations of the resulting velocity fields are considered as outputs. This input-output analysis can in principle be done in any geometry and for the full nonlinear NS equations. In such generality however, it is difficult to obtain useful results. We therefore concentrate on the geometry of channel flows, and the input-output dynamics of the LNS equations.

Our work is greatly influenced by recent research in what has become known as transient growth mechanisms for bypass transitions. We will only briefly outline some of the more closely related work here, and refer the reader to the recent monograph [1] and the references therein for a fuller discussion. The main point of departure of this work from classical linear hydrodynamic stability is the fact that the latter is concerned solely with the existence of exponentially growing modes. In other words, it is essentially an asymptotic analysis of infinite time limits. In certain flows however, transient (finite-time) phenomena appear to play a significant role. While the possibility of transient growth has long been recognized, it is only in the past two decades that effective mathematical methods have been used to analyze it. In [2, 3] initial state with the largest transient energy growth in subcritical flows were discovered using a singular value analysis. These 'worst case' initial states lead to flow structures that resemble streamwise vortices and streaks. A somewhat different analysis is done by computing the pseudo-spectrum rather than the spectrum of the generating dynamics [4], and the most unstable pseudo-spectral modes turn out to be related to streamwise vortices and streaks. A third analysis method [5, 6] studies the most energetic response of the linearized Navier-Stokes equations to stochastic excitation. Yet again, the most energetically excited flow structures appear to resemble streamwise vortices and streaks. The common theme between the three methods is that a certain norm of the perturbed flow state is used (namely kinetic energy density), and the responses with respect to various types of *uncertainties* are analyzed.

Our presentation is organized as follows: in section 2, we give a dynamical description of the flow fluctuations, introduce a notion of a spatio-temporal frequency response and define different frequency response quantities that can be determined based on it. In § 3, we present various portions of the spatio-temporal frequency response for Poiseuille flow at $R = 2000$. Our main aim is to illustrate the input-output resonances from forcing inputs in different directions to different components of the velocity field. These input-output resonances turn out to always resemble streamwise vortices and streaks, and a comparison between them and internal resonances (TS waves) is given using the frequency response. One of our other conclusions is that forcing in the spanwise and wall normal directions is respectively much more influential on flow perturbations than forcing in the streamwise direction. These facts have recently been observed in studies of flow control using the Lorentz force [7, 8, 9]. An analytical explanation for this as well as formulae for the dependence of this influence on the Reynolds number is given in § 4. We conclude by remarking on the utility of input-output analysis, and more generally analysis of effects of uncertainty on transitional and fully turbulent flows and their control.

2 Dynamical description of flow fluctuations

We consider externally excited LNS in channel flow geometry shown in Figure 1. The minimal state-space representation of these equations after application of Fourier transform in spatially invariant directions takes the following form [10]

$$
\begin{aligned}
\partial_t \psi &= \mathcal{A}\psi + \mathcal{B}\mathbf{d}, \\
\phi &= \mathcal{C}\psi,
\end{aligned}
\tag{1}
$$
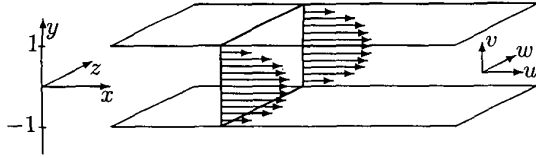
Figure 1: Three dimensional channel flow.

where $\psi := [\begin{array}{cc} v & \omega_y \end{array}]^T$, $\mathbf{d} := [\begin{array}{ccc} d_x & d_y & d_z \end{array}]^T$, and $\phi := [\begin{array}{ccc} u & v & w \end{array}]^T$ represent state, input, and output vector fields, respectively. Each field is assumed to vary both temporally and spatially, e.g. $\mathbf{d} = \mathbf{d}(k_x, y, k_z, t)$. Operators $\mathcal{A}$, $\mathcal{B}$, and $\mathcal{C}$ are given by

$$\mathcal{A} := \begin{bmatrix} \mathcal{A}_{11} & 0 \\ \mathcal{A}_{21} & \mathcal{A}_{22} \end{bmatrix}, \quad \mathcal{B} := [\begin{array}{ccc} \mathcal{B}_x & \mathcal{B}_y & \mathcal{B}_z \end{array}],$$

$$\mathcal{A}_{11} := -ik_x\Delta^{-1}U\Delta + ik_x\Delta^{-1}U'' + \frac{1}{R}\Delta^{-1}\Delta^2,$$

$$\mathcal{A}_{22} := -ik_xU + \frac{1}{R}\Delta,$$

$$\mathcal{A}_{21} := -ik_zU',$$

$$\mathcal{B}_x := \begin{bmatrix} -ik_x\Delta^{-1}\partial_y \\ ik_z \end{bmatrix}, \quad \mathcal{B}_y := \begin{bmatrix} -(k_x^2 + k_z^2)\Delta^{-1} \\ 0 \end{bmatrix},$$

$$\mathcal{B}_z := \begin{bmatrix} -ik_z\Delta^{-1}\partial_y \\ -ik_x \end{bmatrix},$$

$$\mathcal{C} := \begin{bmatrix} \mathcal{C}_u \\ \mathcal{C}_v \\ \mathcal{C}_w \end{bmatrix} := \frac{1}{k_x^2 + k_z^2}\begin{bmatrix} ik_x\partial_y & -ik_z \\ k_x^2 + k_z^2 & 0 \\ ik_z\partial_y & ik_x \end{bmatrix}, \quad (2)$$

where $U(y)$ is a nominal velocity, $U' := dU(y)/dy$, and $\Delta := \partial_y^2 - k_x^2 - k_z^2$. System (1) is parameter-ized by three important parameters: the streamwise wave number k_x, the spanwise wave number k_z, and the Reynolds number R. State of the system is expressed in terms of wall-normal velocity v and vorticity ω_y fields. Streamwise and spanwise velocity components are de-noted by u and w, and forces in the streamwise, wall-normal, and spanwise directions are represented by d_x, d_y, and d_z, respectively. The boundary conditions on v and ω_y are derived from the original no-slip bound-ary conditions and can be written as: $v(k_x, \pm 1, k_z, t) = \partial_y v(k_x, \pm 1, k_z, t) = \omega_y(k_x, \pm 1, k_z, t) = 0$, $\forall k_x, k_z \in \mathbb{R}$, $\forall t \geq 0$.

The *spatio-temporal frequency response* of system (1) is given by

$$\mathcal{H}(k_x, k_z, \omega) = \mathcal{C}(k_x, k_z)(i\omega I - \mathcal{A}(k_x, k_z))^{-1}\mathcal{B}(k_x, k_z),$$

where the frequency response is obtained directly from the Fourier symbols of the operators defining the state space realization. Since $\mathcal{H}$ is a function of three inde-pendent variables there is a variety of different ways to visualize system properties. For example, one can study the maximal singular values of the operator $\mathcal{H}$

$$\bar{\sigma}(\mathcal{H}(k_x, k_z, \omega)) := \{\bar{\lambda}(\mathcal{H}^*(k_x, k_z, \omega)\mathcal{H}(k_x, k_z, \omega))\}^{\frac{1}{2}},$$

or compute the Hilbert–Schmidt norm of $\mathcal{H}$

$$||\mathcal{H}(k_x, k_z, \omega)||_{HS}^2 := \text{trace}(\mathcal{H}^*(k_x, k_z, \omega)\mathcal{H}(k_x, k_z, \omega)).$$

Furthermore, suprema or averages over different fre-quencies can be determined as well, e.g. by computing the temporal-supremum of the maximal singular values of the operator $\mathcal{H}$

$$[||\mathcal{H}||_\infty](k_x, k_z) := \sup_\omega \bar{\sigma}(\mathcal{H}(k_x, k_z, \omega)), \quad (3)$$

or the temporal-average of the Hilbert–Schmidt norm of the operator $\mathcal{H}$

$$[||\mathcal{H}||_2^2](k_x, k_z) := \frac{1}{2\pi}\int_{-\infty}^{\infty} ||\mathcal{H}(k_x, k_z, \omega)||_{HS}^2 \, d\omega. \quad (4)$$

Notation used in (3) and (4) indicates that the cor-responding quantities represent, for any given pair (k_x, k_z), $\mathcal{H}_\infty$ and $\mathcal{H}_2$–norms of system (1), respectively.

For stable systems, the quantity defined by (4) can be determined based on solutions of the operator Lya-punov equations of the form

$$\begin{aligned} \mathcal{A}\mathcal{X} + \mathcal{X}\mathcal{A}^* &= -\mathcal{B}\mathcal{B}^*, \\ \mathcal{A}^*\mathcal{Y} + \mathcal{Y}\mathcal{A} &= -\mathcal{C}^*\mathcal{C}, \end{aligned}$$

as

$$\begin{aligned} [||\mathcal{H}||_2^2](k_x, k_z) &= \text{trace}\{\mathcal{X}(k_x, k_z)\mathcal{C}^*(k_x, k_z)\mathcal{C}(k_x, k_z)\} \\ &= \text{trace}\{\mathcal{Y}(k_x, k_z)\mathcal{B}(k_x, k_z)\mathcal{B}^*(k_x, k_z)\}, \end{aligned}$$

where $\mathcal{A}^*$, $\mathcal{B}^*$, and $\mathcal{C}^*$ represent adjoints of operators $\mathcal{A}$, $\mathcal{B}$, and $\mathcal{C}$, respectively.

It is also relevant to investigate frequency domain prop-erties of the operators that map different components of the external excitation field to the chosen output. By performing analyses of this type, one can derive im-portant conclusions about the effectiveness of an input applied in a certain spatial direction, and relative im-portance of different velocity field components.

Clearly, operator $\mathcal{H}(k_x, k_z, \omega)$ can be represented as

$$\begin{aligned} \mathcal{H} &= \begin{bmatrix} \mathcal{H}_u \\ \mathcal{H}_v \\ \mathcal{H}_w \end{bmatrix} = [\begin{array}{ccc} \mathcal{H}_x & \mathcal{H}_y & \mathcal{H}_z \end{array}] \\ &= \begin{bmatrix} \mathcal{H}_{ux} & \mathcal{H}_{uy} & \mathcal{H}_{uz} \\ \mathcal{H}_{vx} & \mathcal{H}_{vy} & \mathcal{H}_{vz} \\ \mathcal{H}_{wx} & \mathcal{H}_{wy} & \mathcal{H}_{wz} \end{bmatrix}, \quad (5) \end{aligned}$$

where

$$\mathcal{H}_r := \mathcal{C}_r(i\omega I - \mathcal{A})^{-1}\mathcal{B}, \quad r = u, v, w,$$

$$\mathcal{H}_s := \mathcal{C}(i\omega I - \mathcal{A})^{-1}\mathcal{B}_s, \quad s = x, y, z,$$

$$\mathcal{H}_{rs} := \mathcal{C}_r(i\omega I - \mathcal{A})^{-1}\mathcal{B}_s, \quad \left\{\begin{array}{c} r = u, v, w \\ s = x, y, z \end{array}\right\},$$

denote the operator valued transfer functions from $\mathbf{d}$ to r, d_s to ϕ, and d_s to r evaluated on the $i\omega$ axis, respectively.

In this paper we confine our attention to the analysis of the $\mathcal{H}_2$–norm-like quantities for system (1). We note that the analysis of the different portions of the fre-quency responses will shed light on different aspects of system's dynamics. This is illustrated in § 3 where we discuss the results obtained by numerical computations of different notions defined here for Poiseuille flow.

3 Frequency responses in Poiseuille flow

In this section we study the results obtained by computing various $\mathcal{H}_2$–norm–like quantities for the NS equations linearized around a nominal velocity profile of the form $U(y) = 1 - y^2$ at $R = 2000$. All results presented here are obtained numerically using the scheme described in [10], with 30 v and ω_y basis functions. By increasing the number of basis functions it is confirmed that this resolution is high enough. The $\mathcal{H}_2$–norm–like quantities are determined based on solutions of the corresponding Lyapunov equations, with 50×90 grid points in the wave-number space (k_x, k_z). These points are chosen in the logarithmic scale with $\{k_{xmin} := 10^{-4}, k_{xmax} := 3.02\}$ and $\{k_{zmin} := 10^{-2}, k_{zmax} := 15.84\}$.

Plots of

$$\left[\|\mathcal{H}_s\|_2^2 \right] (k_x, k_z) := \frac{1}{2\pi} \int_{-\infty}^{\infty} \|\mathcal{H}_s(k_x, k_z, \omega)\|_{HS}^2 \, d\omega,$$

for $\{s = x, y, z\}$ are shown in Figure 2. These plots clearly illustrate that the external excitations applied in the wall-normal and spanwise directions have much higher influence on the velocity field than the streamwise direction forcing. The explanation for this phenomenon is given in § 4, where we show that the energy of three-dimensional streamwise constant perturbations in the presence of either d_y or d_z achieves $O(R^3)$ amplification. On the other hand, only amplification proportional to the Reynolds number is achievable when external forcing in the streamwise direction is applied, as illustrated in § 4. Since $[\|\mathcal{H}_s\|_2] (k_x, k_z)$ attains largest values in the immediate vicinity of the spanwise wave-number axis, the results of § 4 offer a reasonable answer for a rather limited role of d_x in the process of energy amplification.

Furthermore, both $[\|\mathcal{H}_y\|_2] (k_x, k_z)$ and $[\|\mathcal{H}_z\|_2] (k_x, k_z)$ achieve largest values at the different locations in the (k_x, k_z)–plane than $[\|\mathcal{H}_x\|_2] (k_x, k_z)$. Clearly, the former two quantities peak at $k_x = 0$ for certain non-zero value of k_z. These input-output resonances correspond to the streamwise vortices and streaks and their importance has been studied in great detail by [2, 3, 4, 5, 6], among others. On the other hand, the latter quantity attains the global maximum at the location where both spatial wave-numbers have $O(1)$ values. We also observe a local peak at the streamwise wave-number axis in the left plot. This peak is caused by the least-damped modes of $\mathcal{A}$ (TS waves). Even though the presence of the least-damped modes in the left plot is more prominent than in the middle and right plots, the structures that are more amplified by system's dynamics are still three-dimensional. These structures correspond to the so-called *oblique waves* [1]. The identification of the oblique waves as the input-output resonances illustrates usefulness of the input-output approach to the analysis of the problem at hand.

Figure 3 illustrates a contribution of different components of the velocity field to the overall energy amplification by showing k_x–k_z dependence of the following quantities

$$\left[\|\mathcal{H}_r\|_2^2 \right] (k_x, k_z) := \frac{1}{2\pi} \int_{-\infty}^{\infty} \|\mathcal{H}_r(k_x, k_z, \omega)\|_{HS}^2 \, d\omega,$$

for $\{r = u, v, w\}$. As one can notice, the streamwise velocity plays much bigger role in the process of energy amplification than the other two velocity components. The analytical explanation for this observation is given in § 4, where we explicitly show that the variance of three-dimensional streamwise velocity perturbations at $k_x = 0$ scales as R^3. This is in sharp contrast with the amplification that v and w experience. Namely, our derivations of § 4 prove that the variance of streamwise constant wall-normal and spanwise velocity perturbations is only proportional to the Reynolds number. Moreover, we note that $[\|\mathcal{H}_u\|_2] (k_x, k_z)$, $[\|\mathcal{H}_v\|_2] (k_x, k_z)$, and $[\|\mathcal{H}_w\|_2] (k_x, k_z)$ have their peaks on the k_z-axis, k_x-axis, and at the location in the k_x–k_z plane where both wave numbers are of $O(1)$, respectively. These peaks correspond to streamwise vortices and streaks (left plot), under-damped system modes (middle plot), and oblique waves (right plot). Since the evolution of the wall-normal velocity is governed by the stable Orr-Sommerfeld equation, it is not surprising that $[\|\mathcal{H}_v\|_2] (k_x, k_z)$ achieves largest values in the immediate vicinity of the least-damped modes. On the other hand, both u and w depend on ω_y (cf. (2)), and therefore, they experience transient amplification due to a coupling between wall-normal velocity and vorticity perturbations. Since for streamwise constant perturbations w depends only on v (cf. (2)), the amplification of spanwise velocity perturbations at $k_x = 0$ is limited to $O(R)$, as shown in § 4. Clearly, this amplification becomes larger when non-zero streamwise wave-numbers are considered. This can be attributed to the fact that away from the k_z–axis w is a function of both wall-normal velocity and wall-normal vorticity (cf. (2)). The latter quantity achieves much bigger magnitudes than the former due to the aforementioned coupling between them, and it is responsible for the input-output resonances observed in the far right plot.

The numerical computations of this section are strengthened by a rigorous analysis of the various $\mathcal{H}_2$–norms of the streamwise constant three-dimensional channel flow perturbations. These analytical consideration are presented in § 4.

4 Dependence of $\mathcal{H}_2$–norm on R at $k_x = 0$

In this section, we study system (1) in the presence of streamwise constant three-dimensional perturbations, that is at $k_x = 0$. Our considerations are valid for an arbitrary nominal velocity profile $U(y)$. The motivation for a thorough analysis of this particular case stems from numerical computations presented in § 3 which reveal that the most amplified input-output resonances take place at $k_x = 0$. The results presented here represent a natural continuation of [6].

We first study the $\mathcal{H}_2$–norms of all components of the operator transfer function (5), that is

$$\left[\|\mathcal{H}_{rs}\|_2^2 \right] (k_z) := \frac{1}{2\pi} \int_{-\infty}^{\infty} \|\mathcal{H}_{rs}(k_z, \omega)\|_{HS}^2 \, d\omega,$$

$\{r = u, v, w; \ s = x, y, z\}$. We then investigate the effectiveness of an input applied in a certain spatial direction by studying the Reynolds number dependence

of $\left[\|\mathcal{H}_s\|_2^2\right](k_z)$, for $\{s = x, y, z\}$. Finally, we illustrate the contribution of particular components of the velocity field to the overall energy amplification by doing similar analysis for $\left[\|\mathcal{H}_r\|_2^2\right](k_z)$, with $\{r = u, v, w\}$. By performing analysis of this type, we are able to derive important conclusions about the effectiveness of input field components, and the contributions of the streamwise, wall-normal, and spanwise velocities to the overall energy amplification.

In order to determine the $\mathcal{H}_2$–norm of the operator that maps d_s into r, for every $\{r = u, v, w; \; s = x, y, z\}$, we rewrite system (1) as

$$\begin{aligned} \partial_t \psi &= \mathcal{A}\psi + \mathcal{B}_s d_s, \\ r &= \mathcal{C}_r \psi. \end{aligned} \tag{6}$$

Based on the analysis of the corresponding operator Lyapunov equations we are able to prove the following theorem [11].

Theorem 1 *For any channel flow with nominal velocity $U(y)$, the $\mathcal{H}_2$–norm of system (6) at $k_x = 0$ is given by*

$$\begin{aligned} & \begin{bmatrix} \|\mathcal{H}_{ux}\|_2^2 & \|\mathcal{H}_{uy}\|_2^2 & \|\mathcal{H}_{uz}\|_2^2 \\ \|\mathcal{H}_{vx}\|_2^2 & \|\mathcal{H}_{vy}\|_2^2 & \|\mathcal{H}_{vz}\|_2^2 \\ \|\mathcal{H}_{wx}\|_2^2 & \|\mathcal{H}_{wy}\|_2^2 & \|\mathcal{H}_{wz}\|_2^2 \end{bmatrix} \\ & = \begin{bmatrix} f_{ux}(k_z)R & g_{uy}(k_z)R^3 & g_{uz}(k_z)R^3 \\ 0 & f_{vy}(k_z)R & f_{vz}(k_z)R \\ 0 & f_{wy}(k_z)R & f_{wz}(k_z)R \end{bmatrix}. \end{aligned} \tag{7}$$

The $\mathcal{H}_2$–norm of the streamwise constant perturbations scales as R^3 from the forces in the wall-normal and the spanwise directions to the streamwise velocity. In all other cases it scales as R. In particular, at $k_x = 0$ the streamwise direction forcing does not influence the wall-normal and the spanwise velocity components. This illustrates the dominance of the streamwise velocity perturbations and the forces in the remaining two spatial directions for high Reynolds number channel flows.

The expressions for the terms that multiply R in (7) are the same for all channel flows, as shown in [11]. On the other hand, the expressions for g_{uy} and g_{uz} depend on the coupling operator $\mathcal{A}_{21} := -ik_z U'(y)$, and therefore these terms are nominal-velocity dependent.

In order to determine the influence of various input field components to the entire velocity field we rewrite system (1) as

$$\begin{aligned} \partial_t \psi &= \mathcal{A}\psi + \mathcal{B}_s d_s, \\ \phi &= \mathcal{C}\psi, \end{aligned} \tag{8}$$

with $\{s = x, y, z\}$. We are now able to state the following corollary of Theorem 1.

Corollary 2 *For any channel flow with nominal velocity $U(y)$, the $\mathcal{H}_2$–norm of system (8) at $k_x = 0$ is given by*

$$\begin{aligned} \left[\|\mathcal{H}_x\|_2^2\right](k_z) &= f_x(k_z)R, \\ \left[\|\mathcal{H}_y\|_2^2\right](k_z) &= f_y(k_z)R + g_y(k_z)R^3, \\ \left[\|\mathcal{H}_z\|_2^2\right](k_z) &= f_z(k_z)R + g_z(k_z)R^3, \end{aligned}$$

where

$$\begin{aligned} f_x &:= f_{ux}, \quad f_y := f_{vy} + f_{wy}, \quad f_z := f_{vz} + f_{wz}, \\ g_y &:= g_{uy}, \quad g_z := g_{uz}. \end{aligned}$$

Figure 4 graphically illustrates the k_z–dependence of functions f_x, f_y, f_z, g_y, and g_z. Expressions for f_x, f_y, and f_z are the same for all channel flows, as shown in [11] where the analytical formulae for these quantities have been derived. On the other hand, both g_y and g_z depend on the nominal velocity. In [11], the analytical expressions for these two quantities in Couette flow have been determined by doing the spectral decompositions of the Orr-Sommerfeld and Squire operators. These expressions are given in terms of rapidly convergent series and they are shown in the middle plot of Figure 4. The numerically computed dependence of g_y and g_z on k_z in Poiseuille flow is given in the right plot of the same figure.

Therefore, as already indicated by the numerical computations of § 3, the forces in the spanwise and wall-normal directions have the strongest influence on the velocity field. This observation is consistent with recent work on channel flow turbulence control using the Lorentz force [7, 8, 9], where it was concluded that forcing in the spanwise direction had the strongest effect in suppressing turbulence. We confirmed this observation by analytical derivations for the streamwise constant perturbations showing that the square of the $\mathcal{H}_2$–system–norm from d_z and d_y to velocity vector ϕ scales as R^3. On the other hand, at $k_x = 0$, the square of the $\mathcal{H}_2$–norm from d_x to ϕ scales as R.

For a system of the form

$$\begin{aligned} \partial_t \psi &= \mathcal{A}\psi + \mathcal{B}\mathbf{d}, \\ r &= \mathcal{C}_r \psi, \end{aligned} \tag{9}$$

with $\{r = u, v, w\}$, we state the following corollary of Theorem 1.

Corollary 3 *For any channel flow with nominal velocity $U(y)$, the $\mathcal{H}_2$–norm of system (9) at $k_x = 0$ is given by*

$$\begin{aligned} \left[\|\mathcal{H}_u\|_2^2\right](k_z) &= f_u(k_z)R + g_u(k_z)R^3, \\ \left[\|\mathcal{H}_v\|_2^2\right](k_z) &= f_v(k_z)R, \\ \left[\|\mathcal{H}_w\|_2^2\right](k_z) &= f_w(k_z)R, \end{aligned}$$

where

$$\begin{aligned} f_u &:= f_{ux}, \qquad g_u := g_{uy} + g_{uz}, \\ f_v &:= f_{vy} + f_{vz}, \quad f_w := f_{wy} + f_{wz}. \end{aligned}$$

Figure 5 graphically illustrates the k_z–dependence of functions f_u, f_v, f_w, and g_u. Expressions for f_u, f_v, and f_w are the same for all channel flows, as shown in [11] where the analytical formulae for these quantities have been derived. On the other hand, g_u depends on the underlying mean velocity. In [11], the analytical dependence of g_u on k_z for Couette flow has been derived. The right plot in Figure 5 shows the numerically computed k_z–dependence of g_u in Poiseuille flow.

Thus, the impact of the external excitations is most powerful on the streamwise velocity component. We confirmed this observation by both numerical computations of § 3 and analytical derivations summarized in Corollary 3 for the streamwise constant perturbations showing that the square of the $\mathcal{H}_2$–system–norm from **d** to u scales as R^3. On the other hand, at $k_x = 0$, the square of the $\mathcal{H}_2$–norm from **d** to v and w scales as R.

It is worth noting that Theorem 1 of [6] follows from Theorem 1 of this section. For completeness, we state the main result of [6] as the following corollary.

Corollary 4 *For any channel flow with nominal velocity $U(y)$, the $\mathcal{H}_2$–norm of system (1) at $k_x = 0$ is given by*

$$\left[\|\mathcal{H}\|_2^2 \right](k_z) \quad = \quad f(k_z)R \quad + \quad g(k_z)R^3,$$

where

$$f \quad := \quad f_{ux} + f_{vy} + f_{vz} + f_{wy} + f_{wz},$$
$$g \quad := \quad g_{uy} + g_{uz}.$$

5 Concluding Remarks

The main objective of the present study has been to analyze the LNS equations from an input-output point of view. In particular, we have investigated the spatio-temporal frequency responses of these equations. The starting point of our study has been an evolution model where the LNS equations are subject to body forces that model external excitations. We have analyzed this forced evolution model both numerically and analytically by deriving the exact formulae for particular frequency response quantities. We have shown that under external excitations, the input-output resonances of the equations occur at different spatio-temporal frequencies than the 'under-damped modes' of the system. These under-damped modes represent TS waves, while the input-output resonances are related to the streamwise vortices and streaks and oblique waves, which are ubiquitous in both transitional channel and boundary layer flows.

The analytical derivations presented in § 4 indicate that all channel flows with a streamwise direction mean velocity that depends only on the wall-normal coordinate are almost alike. This is an important discovery which, for example, indicates that the perturbations around laminar and turbulent wall-bounded flows should act in a similar way. However, the interpretation for these two cases is different. While the laminar flow perturbations initiate transition and consequently lead to turbulence, their turbulent flow counterparts are primarily responsible for sustenance of the turbulent state. Regardless of the interpretation, our results underscore the importance of non-modal effects in both transitional and fully turbulent channel flows.

From control point of view the current work can be considered as a *control oriented modelling*. We have shown that input-output analysis of the LNS equations in the frequency domain has significant implications for control of both transitional and fully turbulent channel flows. With regard to passive control strategies,

our results indicate the spatial directions in which the application of external body forces is most effective. Furthermore, our analysis identifies the dominant flow structures and the regions in the frequency space corresponding to these structures. This represents an important information for the application of feedback control. Arguably, once the phenomena responsible for the transition to turbulence have been properly identified, modelled, and the control objective defined accordingly, feedback control design will be much more likely to give satisfactory results at much higher Reynolds numbers than currently possible [12, 13].

References

[1]   P. J. Schmid and D. S. Henningson, *Stability and Transition in Shear Flows*. New York: Springer-Verlag, 2001.

[2]   K. M. Butler and B. F. Farrell, "Three-dimensional optimal perturbations in viscous shear flow," *Physics of Fluids A*, vol. 4, p. 1637, 1992.

[3]   S. C. Reddy and D. S. Henningson, "Energy growth in viscous channel flows," *J. Fluid Mech.*, vol. 252, pp. 209–238, 1993.

[4]   L. N. Trefethen, A. E. Trefethen, S. C. Reddy, and T. A. Driscoll, "Hydrodynamic stability without eigenvalues," *Science*, vol. 261, pp. 578–584, 1993.

[5]   B. F. Farrell and P. J. Ioannou, "Stochastic forcing of the linearized Navier-Stokes equations," *Physics of Fluids A*, vol. 5, no. 11, pp. 2600–2609, 1993.

[6]   B. Bamieh and M. Dahleh, "Energy amplification in channel flows with stochastic excitation," *Physics of Fluids*, vol. 13, no. 11, pp. 3258–3269, 2001.

[7]   T. W. Berger, J. Kim, C. Lee, and J. Lim, "Turbulent boundary layer control utilizing the Lorentz force," *Physics of Fluids*, vol. 12, no. 3, pp. 631–649, 2000.

[8]   Y. Du and G. E. Karniadakis, "Suppressing wall turbulence by means of a transverse traveling wave," *Science*, vol. 288, pp. 1230–1234, 2000.

[9]   Y. Du, V. Symeonidis, and G. E. Karniadakis, "Drag reduction in wall-bounded turbulence via a transverse travelling wave," *J. Fluid Mech.*, vol. 457, pp. 1–34, 2002.

[10]   M. R. Jovanović and B. Bamieh, "The spatio-temporal impulse response of the linearized Navier-Stokes equations," in *Proceedings of the 2001 American Control Conference*, pp. 1948–1953, 2001.

[11]   M. R. Jovanović and B. Bamieh, "Component-wise energy amplification in channel flows," *Submitted to J. Fluid Mech.*, 2003.

[12]   M. Högberg, T. R. Bewley, and D. S. Henningson, "Linear feedback control and estimation of transition in plane channel flow," *Submitted to J. Fluid Mech.*, 2002.

[13]   K. H. Lee, L. Cortelezzi, J. Kim, and J. Speyer, "Application of reduced-order controller to turbulent flows for drag reduction," *Physics of Fluids*, vol. 13, no. 5, pp. 1321–1330, 2001.
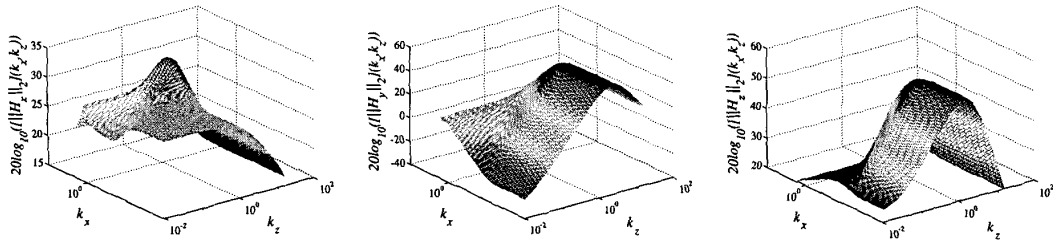
Figure 2: Plots of $[\|\|\mathcal{H}_x\|_2]$ (k_x, k_z), $[\|\|\mathcal{H}_y\|_2]$ (k_x, k_z), and $[\|\|\mathcal{H}_z\|_2]$ (k_x, k_z), in Poiseuille flow with $R = 2000$.
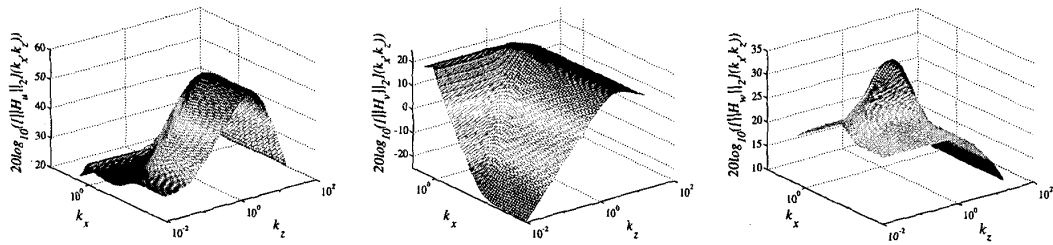
Figure 3: Plots of $[\|\|\mathcal{H}_u\|_2]$ (k_x, k_z), $[\|\|\mathcal{H}_v\|_2]$ (k_x, k_z), and $[\|\|\mathcal{H}_w\|_2]$ (k_x, k_z), in Poiseuille flow with $R = 2000$.
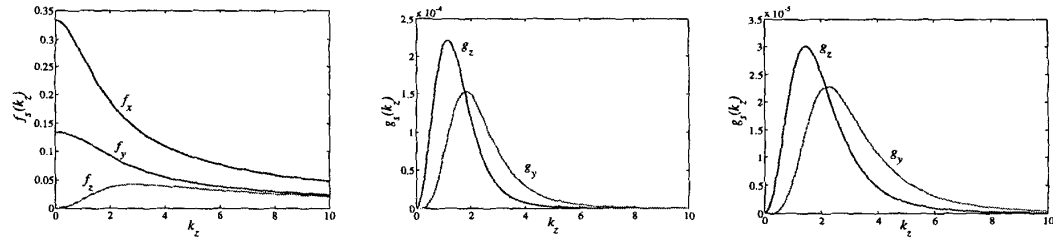
Figure 4: The k_z-dependence of f_x, f_y, f_z, g_y, and g_z. Expressions for f_x, f_y, and f_z are the same for all channel flows, as demonstrated in [11]. The terms responsible for the $O(R^3)$ energy amplification are shown in the middle (Couette flow) and right (Poiseuille flow) plots.
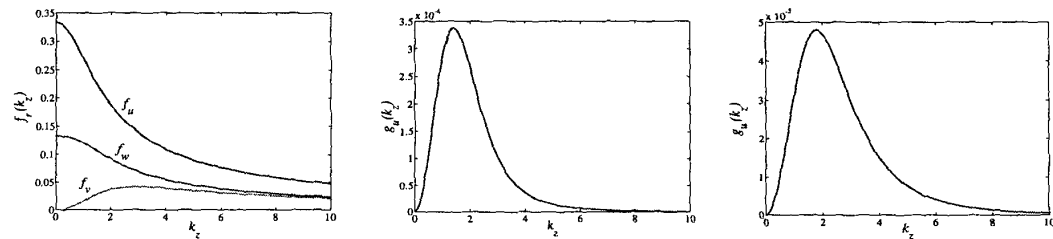
Figure 5: The k_z-dependence of f_u, f_v, f_w, and g_u. Expressions for f_u, f_v, and f_w are the same for all channel flows, as demonstrated in [11]. The terms responsible for the $O(R^3)$ energy amplification are shown in the middle (Couette flow) and right (Poiseuille flow) plots.